PROCEEDINGS OF SPIE

Modelling radiation and energy balances with Landsat 8 images under different thermohydrological conditions in the Brazilian semi-arid region

Antônio H. de C. Teixeira, Janice F. Leivas, Ricardo G. Andrade, Fernando B. T. Hernandez, Franco R. A. Momesso

SPIE.

Modelling radiation and energy balances with Landsat 8 images under different thermohydrological conditions in the Brazilian semi-arid region

Antônio H. de C. Teixeira[*a], Janice F. Leivas[a], Ricardo G. Andrade[a], Fernando B. T. Hernandez[b], Franco R. A. Momesso[b]

[a]Embrapa Satellite Monitoring, Campinas, São Paulo, Brazil; [b]São Paulo State University, Ilha Solteira, São Paulo, Brazil.

ABSTRACT

Four Landsat 8 images were used together with a net of seven agro-meteorological stations for modelling the large-scale radiation and energy balances in the mixed agro-ecosystems inside a semi-arid area composed by irrigated crops and natural vegetation of the Petrolina municipality, Northeast Brazil, along the year 2014. The SAFER algorithm was used to calculate the latent heat flux (λE), net radiation (R_n) was acquired by the Slob equation, ground heat flux (G) was considered as a fraction of R_n and the sensible flux (H) was retrieved by residue in the energy balance equation. For classifying the vegetation into irrigated crops and natural vegetation, the SUREAL algorithm was applied to determine the surface resistance (r_s) and threshold values for r_s were used to characterize the energy fluxes from these types of vegetated surfaces. Clearly one could see higher λE from irrigated crops than from natural vegetation with some situations of heat horizontal advection increasing its values until 23% times larger than R_n, with respective average λE ranges of 5.7 (64% of R_n) to 7.9 (79% of R_n) and 0.4 (4% of R_n) to 4.3 (37% of R_n) MJ m^{-2} d^{-1}. The corresponding H mean values were from 1.8 (18% of R_n) to 3.2 (28% of R_n) and 5.4 (60% of R_n) to 9.2 (94% of R_n) MJ m^{-2} d^{-1}. Average G pixel values ranged from 0.3 to 0.4 MJ m^{-2} d^{-1}, representing 3 and 4% of R_n for natural vegetation and irrigated crops, respectively.

Keywords: net radiation, latent heat flux, sensible heat flux, soil heat flux, energy partition.

1. INTRODUCTION

The municipality of Petrolina, Pernambuco state, located in the Brazilian semi-arid region, is nowadays, an important agricultural growing region, because of the irrigation technologies applied to fruit crops, at the vicinities of the São Francisco River. Under the rapid land use-changing conditions, the use of remote sensing by satellite images is highly relevant for quantification the energy exchanges on large scales, what has been used in distinct environments[1-4].

Remote sensing by satellite images together a Geographic Information System (GIS) is a suitable way for determining and mapping the spatial and temporal structure of the radiation and energy balance components. Several algorithms have been developed for this task on a large scale, highlighted by some advantages and shortcomings, as for example, the Surface Energy Balance Algorithm for Land—SEBAL[5], the Surface Energy Balance Index—S-SEBI[6] and the Surface Energy Balance System—SEBS[7]. They can be applied to various agro-ecosystems without the need of crop classification, considered difficult in mixed agro-ecosystems.

One of the disadvantages of some remote sensing radiation and energy balance methods is the need to identify extreme hydrological conditions in the satellite images what is difficult during rainy conditions. This is not required for applications

[*]heriberto.teixeira@embrapa.br; Phone 55 19 3211-6200; Fax: 55 19 3211-6222; www.cnpm.embrapa.br

of the Two-Source Model—TSM[8], Dual-Temperature Difference—DTD[9] and Disaggregated Atmosphere Land Exchange Inverse model—DisALEXI[10]. In the aerodynamic resistance-surface energy balance approach—RSEB[11] small errors in the radiative temperature translate into large inaccuracies in the sensible heat flux (H), and then into estimates of latent heat flux (λE).

Other problem in relation to the applicability of the remote sensing radiation and energy balance models, aiming at the end users, is the need of background knowledge in radiation physics involved. The suitability of applying the Penman-Monteith (PM) equation by the surface conductance algorithm has showed with the use of remotely sensed vegetation indices (leaf area index and NDVI) together with weather data[12]. Yet, the strongest advantage of the PM equation is its applicability and the low sensitivity to input data and parameters, being also highlighted by the METRIC (Mapping Evapotranspiration with High Resolution and Internalized Calibration) model[13].

Although the worldwide known SEBAL (Surface Energy Balance Algorithm for Land) algorithm had been calibrated and validated with field radiation and energy balance measurements, presenting a good performance in the Brazilian semi-arid region[14-15], the major difficult for its applicability for the whole year is to select null λE values from the supposed driest pixels in the scenes. During the rainy season, the mixed agro-ecosystems of irrigated crops and natural vegetation are homogenously wet all presenting high water fluxes, with λE values from natural species being even higher than those from irrigation plots[16].

Two algorithms were developed and validated under the Brazilian semi-arid conditions[16]. The SAFER (Simple Algorithm For Evapotranspiration Retrieving) to acquire λE and the SUREAL (Surface Resistance Algorithm) for estimation of the surface resistance to the water fluxes (r_s). This last model has allowed the classification of irrigated crops and natural vegetation in the mixed agro-ecosystems. The algorithms have been successfully applied with Landsat 5/7 and MODIS images[1,16], but not with Landsat 8 (L8) satellite images, yet.

L8 was launched on February 11, 2013 and normal operations started on May 30, 2013. It has a 16-day ground track repeat cycle with an equatorial crossing time at 10:00 a.m. The Operational Land Imager (OLI) on L8 is a nine-band push broom scanner with a swathwidth of 185 km[17]. Despite several radiation and energy balance studies with satellites having different spatial and temporal resolutions have been done, new researches are needed with applications of this new satellite to evaluate these balances, especially for operational energy exchanges monitoring in different agro-ecosystems under rapid land-use changes and having high temporal and spatial thermohydrological variations.

The objective of the current work was to apply the SAFER and SUREAL algorithms with L8 images together with a net of agrometeorological stations aiming the large-scale energy radiation and energy balance components quantifications. The semi-arid area study area is composed by mixed agro-ecosystems of irrigated crops and natural vegetation, close to the São Francisco River, inside the Petrolina municipality, Pernambuco state, Brazilian Northeast. The results can subsidize criteria for political decisions when aiming a rational water resources management in conditions of rapid land-use, climate changes and water competitions by different sectors. The success of the modelling here with the new L8 satellite may give more confidence for the test and validations in other environments around the world, which probably will need only calibrations of the original equations.

2. MATERIAL AND METHODS

2.1. *Study area and data set*

Fig. 1 shows the location of the semi-arid study area (dashed red square) inside the Petrolina municipality, Pernambuco (PE) state, Northeast of Brazil, together with the net of seven agrometeorological stations used for the weather data interpolation processes in a GIS environment.
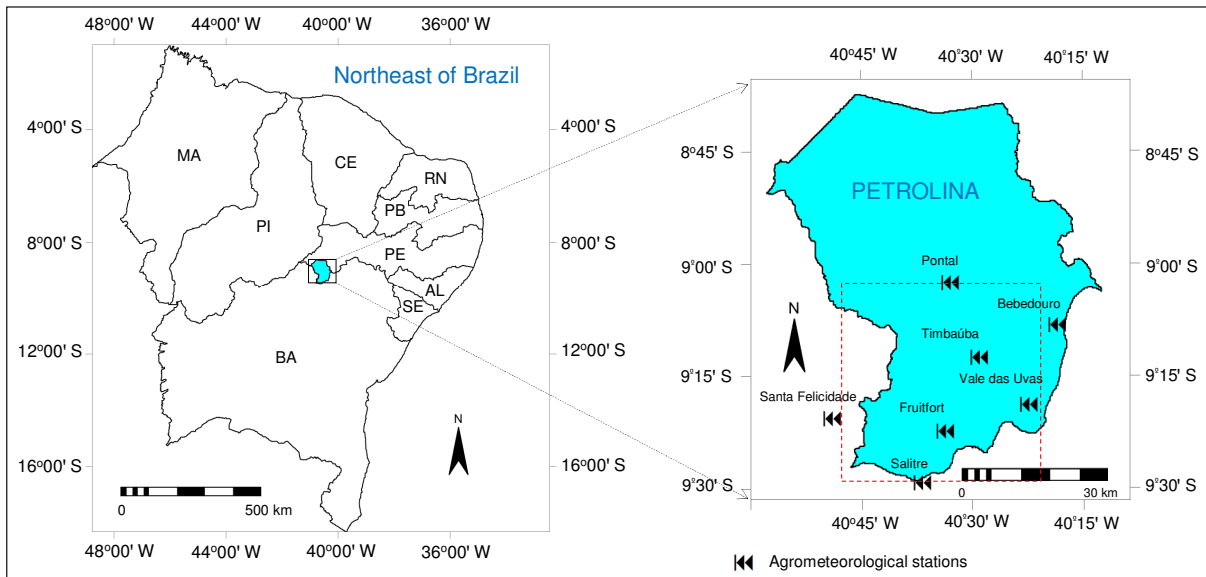
Figure 1. Location of the semi-arid study area (dashed red square on the right side) inside the Petrolina municipality, Pernambuco (PE) state, Northeast Brazil, and the agrometeorological stations used for the weather data interpolation processes in a Geographic Information System (GIS) environment.

In the study area showed in Fig. 1, disturbed currents from the South, North, East and West influence the climatology. Excluding the high-altitude places, all areas present long-term annual air temperature (T_a) higher than 24 °C. The average maximum value is 33 °C and its minimum is 19 °C. The warmest months are October and November when the sun is around the zenith position with low cloud cover while the coldest ones are June and July at the winter solstice in the South hemisphere. The thermal homogeneity strongly contrasts with the spatial and temporal heterogeneity of the precipitation regime. Most rains fall during the first four months of the year, accounting for 68% of the total annual, which presents a long-term (50 years) of 570 mm yr^{-1}. The sandy soil is classified as Latossoil Red-Yellow with low retention capacity, with the groundwater depth around 2.5 m[18].

Mainly fruit crops compose the irrigated agro-ecosystems with the main ones being grapes, mangos, guava and bananas, surrounded by natural vegetation called "Caatinga". This last type of ecosystem is defined as bushes that possess small leaves or thorns. During the dry period it is characterized by senescent vegetation, however, as soon as the rainy season starts, the plants rapidly turn green. Some of the natural species lose their leaves in the dry periods and others store water, being adapted to tolerate water stress, under environmental constraints, which increases rainfall use efficiency[18].

Data from seven agrometeorological stations (see Fig. 1) were used together with 4 L8 images acquired under different thermohydrological conditions along the year 2014 (Day of the Year − DOY: 025 – January, 25; 153 – June, 02; 217 – August, 05; and 265 – September, 22). Grids of global solar radiation (R_G), T_a and reference evapotranspiration (ET_0) were used together with the remotely sensed retrieved parameters during the steps for the large-scale radiation and energy balance components estimations[16].

2.2. *Large-scale radiation and energy balance modeling*

Fig. 2 presents the flowchart for the radiation and energy balance on large-scale by using L8 images and agrometeorological data throughout the SAFER algorithm. The bands 1 to 7 of the L8 sensor were used for the surface albedo (α_0) calculation (spatial resolution of 30 m), while for the surface temperature (T_0), this was done with the bands 10 and 11 (spatial resolution of 100 m).
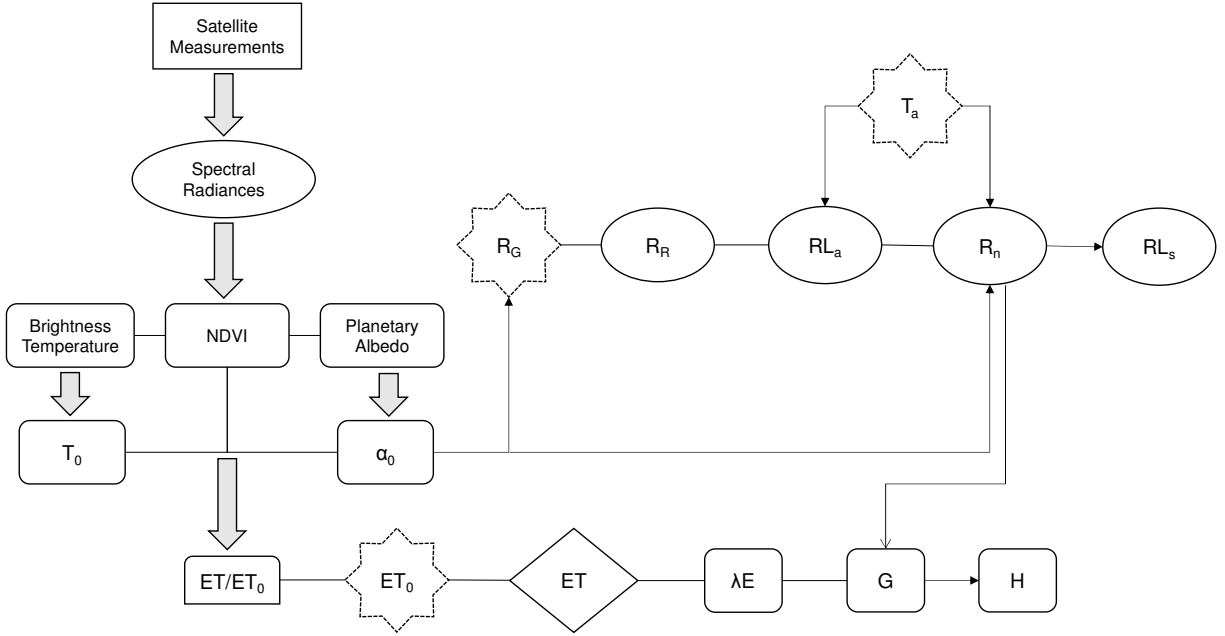
Figure 2. Flowchart for the radiation and energy balances on large-scale by applying the SAFER (Simple Algorithm For Evapotranspiration Retrieving).

Following Fig. 1, the spectral radiances (L_b) were computed from Digital Numbers (DN):

$$L_b = Gain \ x \ DN + Offset \tag{1}$$

where Gain and Offset refer to the values given in the metadata file[17].

The planetary albedo for each Landsat satellite band (αp_b) was calculated as:

$$\alpha p_b = \frac{L_b \pi d^2}{Ra_b \cos \varphi} \tag{2}$$

where L_b is the spectral radiance for the wavelengths of band b (W m^{-2} sr^{-1} µm^{-1}), d is the relative earth-sun distance; Ra_b is the mean solar irradiance at the top of the atmosphere (or atmospheric irradiance) for each band (W m^{-2} µm^{-1}) and φ the solar zenith angle[16].

Ra_b for each of the bands 1 to 7 of the L8 sensor was calculated according to the Planck's low, integrating the radiation over the wavelength intervals and considering its fraction over the solar spectrum, assuming the sun as a blackbody. Then, the broadband planetary albedo (α_p) was calculated as the total sum of the different narrow-band αp_b values according to the weights for each band (w_b).

$$\alpha p = \sum w_b \alpha p_b \tag{3}$$

where the w_b values were computed as the ratio of the amount of the incoming shortwave radiation from the sun at the top of the atmosphere in a particular band and the sum for all the bands.

Table 1 shows the wavelengths, Ra_b and w_b for each of the bands used (B1-B7) for α_p calculations from L8 measurements.

Table 1. Radiometric parameters for the planetary albedo (α_p) calculations with Landsat 8 (L8) images: wavelengths for the bands − λ_b; mean solar irradiance at the top of the atmosphere for each band − Ra_b; and the weights for each band − w_b.

L8 Parameter	B1	B2	B3	B4	B5	B6	B7
λ_b (μm)	0.43-0.45	0.45-0.51	0.53-0.59	0.64-0.67	0.85-0.88	1.57-1.65	2.11-2.29
Ra_b (W m^{-2} μm^{-1})	1718.8	1810.4	1741.7	1558.3	962.5	206.3	68.8
w_b	0.10	0.31	0.30	0.13	0.08	0.05	0.04

The spectral radiances from the bands 10 (L_{10}) and 11 (L_{11}) from the L8 thermal regions were converted into radiometric temperatures applicable at the top of the atmosphere (T_b) by inversion of the Plank's law in the 10.6–11.19 μm (band 10) and 11.5–12.51 μm (band 11) bandwidth:

$$T_b = \frac{K_2}{\ln(\frac{K_1}{L_b+1})} \qquad (4)$$

where K_1 (774.89 and 480.89) and K_2 (1321.08 and 1201.14) for bands 10 and 11, respectively, are conversion coefficients for the L8 satellite. The average T_b value from the two bands was considered the brightness temperature (T_{bright}).

The results for both α_p and T_{bright} were corrected atmospherically for acquiring the albedo (α_0) and temperature (T_0) surface values, by regression equations obtained from satellite and field measurements in the Brazilian semi-arid region[1,14,16].

NDVI is an indicator related to the land cover obtained from satellite images as:

$$NDVI = \frac{\alpha p_{(nir)} - \alpha p_{(red)}}{\alpha p_{(nir)} + \alpha p_{(red)}} \qquad (5)$$

where αp_{nir} and αp_{red} represent the planetary albedo over the ranges of wavelengths in the near infrared (subscript *nir*) and red (subscript *red*) regions of the solar spectrum, which For L8 satellite were B5 and B4, respectively (see Table 1)

Daily R_n was calculated by using the Slob equation:
$$R_n = (1-\alpha_0)R_G - a_L \tau_{sw} \qquad (6)$$

where the regression coefficient a_L was spatially distributed through its relationship with T_a[19].

$$a_L = aT_a - b \qquad (7)$$

and a and b are regression coefficients[14] found to be 6.99 and 39.93. A constant value for $a_L = 110$ was previously used without considering the spatial thermal differences[5].

The atmospheric longwave radiation (RL_a) was calculated based on the physic concepts of the Stefan-Boltzmann low:
$$RL_a = \sigma\ \varepsilon_A T_a^4 \qquad (8)$$

where ε_A was calculated as follows[1,16,18-19]:

$$\varepsilon_A = a_A(-\ln\tau)^{b_A} \qquad (9)$$

where τ is the short-wave atmospheric transmissivity calculated as the ratio of R_G to the incident solar radiation at the top of the atmosphere and a_A and b_A are regression coefficients 0.94, and 0.11, which are in between those for Idaho[20] ($a_A = 0.85$ and $b_A = 0.09$) and for Egypt[5] ($a_A = 1.08$ and $b_A = 0.26$).

Estimating the reflected solar radiation (R_R) as the product of R_G by α_0, the longwave surface radiation (RL_s) was retrieved as residue in the radiation balance equation:
$$R_R = \alpha_0 R_G \qquad (10)$$

$$RL_s = R_G - R_R + RL_a - R_n \tag{11}$$

The instantaneous values of the ratio ET/ET_0 were modelled and multiplied by the grids of ET_0 from the agrometeorological stations (see Fig. 1) for estimating the daily ET large-scale values[16,21-22] and then transformed into energy units to give λE:

$$\frac{ET}{ET_0} = \exp\left[a_S + b_S\left(\frac{T_0}{\alpha_0 NDVI}\right)\right] \tag{12}$$

where ET_0 was calculated by Penman-Monteith's method[23], and a_s and b_s are the regression coefficients 1.8 and -0.008, respectively, for the Brazilian semi-arid conditions.

Eq. 12 does not work for water bodies, i.e. when $NDVI < 0$. Thus, the concept of equilibrium evapotranspiration (ET_{eq})[24] is adopted under these conditions in the SAFER algorithm, and λE_{eq} is retrieved throughout conditional functions applied to the NDVI values as:

$$\lambda E_{eq} = \frac{s\ (R_n - G)}{s + \gamma} \tag{13}$$

where s is the slope of the curve relating saturation water vapor pressure to T_a, G is the ground heat flux and γ is the psychometric constant. Under these conditions, as the surface moisture availability is not constrained, water vapor transfer is only limited by the available energy.

For the daily G values, the following equation was used[1,16,21-22]:

$$\frac{G}{R_n} = a_G \exp(b_G \alpha_0) \tag{14}$$

where a_G and b_G are regression coefficients found to be 3.98 and -25.47, respectively for the Brazilian semi-arid conditions.

The sensible heat flux (H) was estimated as residue in the energy balance equation[22]:

$$H = R_n - \lambda E - G \tag{15}$$

For classification of the vegetated surface into irrigated crops and natural vegetation, the SUREAL (Surface Resistance Algorithm) model was applied[25]:

$$r_s = \exp\left[a_r\left(\frac{T_0}{\alpha_0}\right)(1 - NDVI) + b_r\right] \tag{16}$$

where a_r and b_r are regression coefficients, considered respectively 0.04 e 2.72 for the Brazilian Northeast conditions. Pixels with r_s values bellow 800 s m^{-1} and NDVI above or equal to 0.40 were considered as irrigated crops. If r_s was in between 1000 and 10000 s m^{-1} they should be natural vegetation. The high end of this last range was used to eliminate human-built structures.

3. RESULTS AND DISCUSSION

3.1 Weather drivers

The weather-driving forces for the radiation and energy balances are R_G, precipitation (P), and the atmospheric demand represented by ET_0. The trends of these parameters were analysed on a daily scale, during the transition periods comprising the start of the rainy season in 2013 to the its end in 2014, involving the previous, actual and post thermohydrological conditions for the satellite image acquisitions dates (January 2014 to September 2014). Fig. 2 shows their trends in terms of DOY, with weather data from the Timbaúba agrometeorological station (see Fig. 1).
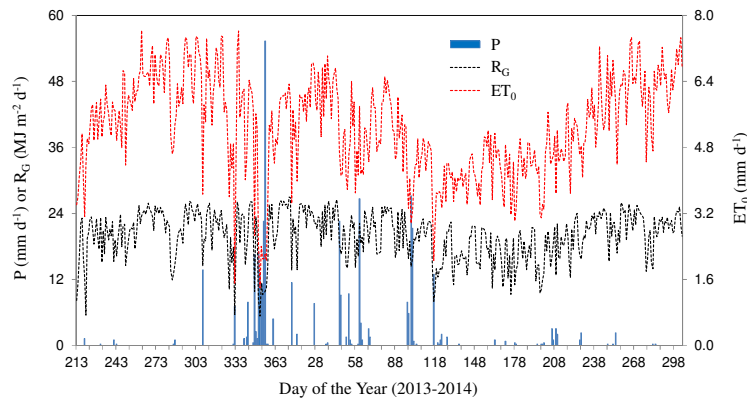
Figure 3. Daily values of precipitation (P), incident global solar radiation (R_G) and reference evapotranspiration (ET_0), involving the days of the year (DOY) from the start of the rainy period in November/2013 to the end of the dry period in October/2014, in the semi-arid study area of Petrolina municipality, Brazilian Northeast region.

P was the most variable weather parameter. The concentrations of rains were from DOY/Year 303/2013 to 120/2014, mainly during the end of 2013. These high moisture conditions affected the energy partition with larger λE and low H in the image of 25 January 2014. The naturally driest periods involving the satellite images were from DOY 210 to 300 of 2014. From the ET_0 daily values, the largest atmospheric demands involving the image dates happened between DOY 242 and 304 of 2014, when they reached to 7.0 mm d^{-1}. In these situations, the sun was in the zenith position with low cloud cover. The R_G daily values were higher than 25 MJ m^{-2} d^{-1} at the end of the years, and bellow 10 MJ m^{-2} day^{-1} in the middle of 2014, with the highest levels related to the sun astronomical position. Under conditions of high P, ET_0 and R_G, both natural vegetation and agricultural crops were in favour for large λE.

3.2 Remote sensing input parameters

The radiation balance among the different kind of vegetation depends on the surface albedo (α_0), the Normalized Difference Vegetation Index (NDVI) and the surface temperature (T_0). α_0 determines the short wave radiation that come back from the vegetated surface to the lower atmosphere; NDVI is a key remote sensing indicator related to the land cover and soil moisture conditions; and the emitted longwave radiation from the surface is directly proportional to T_0.

The spatial distribution of the remote sensing input parameters daily values in the semi-arid study area of Petrolina municipality, Brazilian Northeast, are shown in Fig. 4.
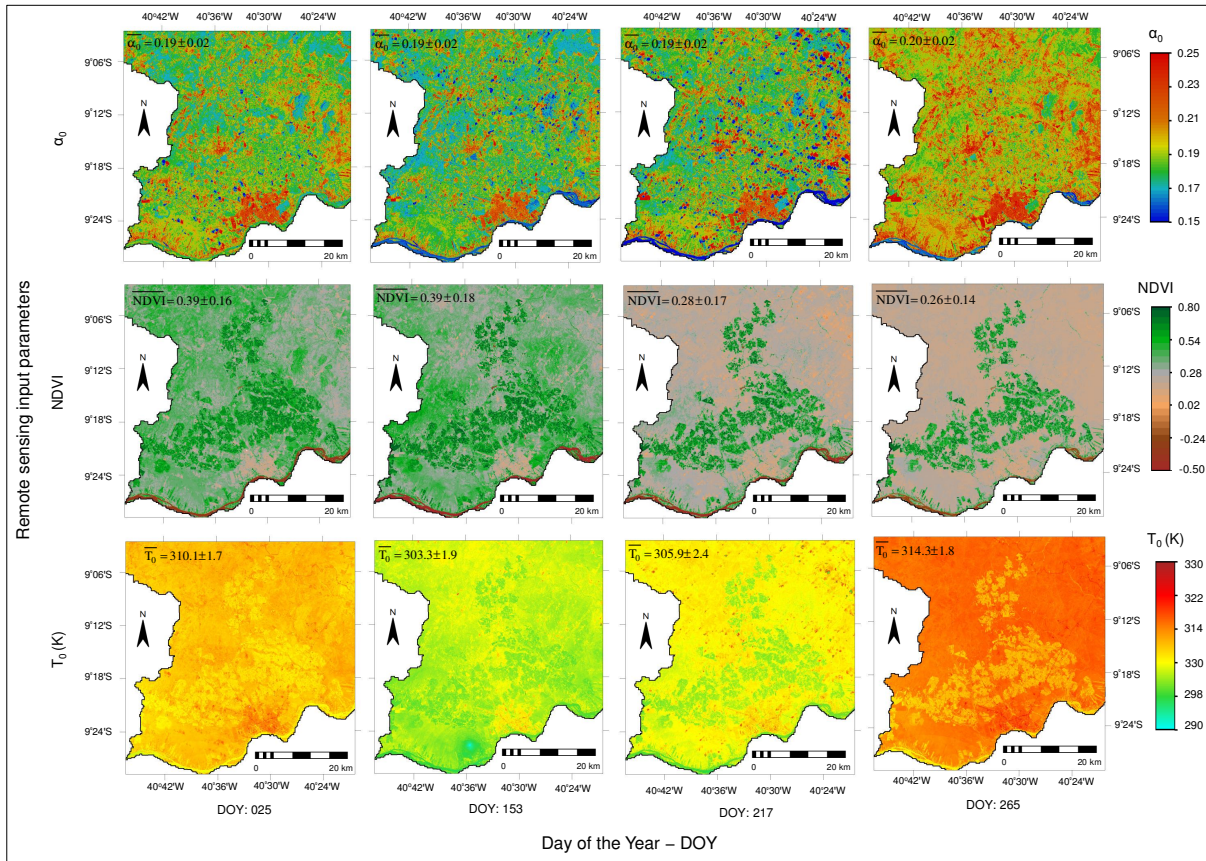
Figure 4. Spatial distribution of the daily values for the remote sensing input parameters in the semi-arid study area of Petrolina (PE) municipality, Brazilian Northeast. Surface albedo (α_0); Normalized Difference Vegetation Index (NDVI); and surface temperature (T_0). Overbars mean average pixel values.

A dark land surface, i.e. with low α_0, absorbs more solar radiation, and has a higher available energy than a bright one. Yet, α_0 also depends on the soil moisture conditions[19,26-27]. The highest values occurred for the image of DOY 265, representing the driest period of the year, because of the coupled effect of low large-scale soil moisture, scarce cloud cover and Sun astronomical position, proportioning large R_G levels. However, the α_0 spatial variations were homogeneous during the different periods of the year with standard deviation (SD) of 0.02 in all images, with no strong distinctions between irrigated crops and natural vegetation. Clearly one can see the largest α_0 values in the southern part of the study area, where Petrolina city is located, close to the São Francisco River. Values for α_0 were reported to be between 0.15 and 0.26, for tropical natural vegetation[28], however the values in the current study are higher than those previously reported for humid tropical regions[29-31]. The relation of α_0 with environmental and moisture conditions is also in accordance with other more recent studies[16,22,26-27,32].

The distinctions among the NDVI large-scale values along the year and between irrigated crops and natural vegetation are much clear than in the case of α_0, with the highest agro-ecosystem differences under the driest conditions in the end of September (DOY 265). On the one hand, the largest averaged pixel values are from January to June, represented by the images of DOY 025 and 153 because the natural vegetation species ("Caatinga") consume water from the first rains, promoting a large increment of biomass (BIO). As there is a relation between λE and BIO[33], the water flux rates are high in irrigated crops than for natural species. Irrigated corn crop presented twice BIO values when compared with natural alpine meadow in the Heithe River Basin, being irrigation considered the main reason for these strong differences[34]. Simultaneously with high R_G levels, irrigated crops are well developed, because the regular irrigation water supply. On the other hand, the lowest large-scale NDVI mean values are observed in September (DOY 265), when after the rainy period, the soil in the root zone of the natural species is dry, promoting their senescence stages.

T_0 affects the energy available, by interfering in the long wave radiation balance, with lower values under irrigation conditions than those for dry areas. However, even differentiating the agro-ecosystems better than α_0 this distinction is not as strong as that for NDVI. One reason for this is the lower spatial resolution of the thermal band (100 m) comparing with the visible ones (30 m) of the L8 sensor. In general, the periods with the highest T_0 values coincided with those with the largest R_G levels (DOY 025 and 265). The lowest ones occurred in the middle of the year, after the rainy season (DOY 153), with the reduction being explained by the soil moisture uniformity in the root zones of the mixed agro-ecosystems together with the winter solstice time in the South hemisphere.

The variability of α_0, NDVI, and T_0 in the "Caatinga" can mainly be attributed to variations in R_G and surface moisture conditions due to Sun position, cloud cover and rainfall. However, for irrigated crops, as the water is in general regularly applied, the variations of these remote sensing parameters, besides the R_G levels, are influenced by the different crop stages together with water and fertilization managements.

3.3 Large-scale radiation balance

The mean daily pixel values of the radiation balance for irrigated crops (IC) and natural vegetation (NV) in the semi-arid study area, involving different conditions along the year 2014 in Petrolina municipality, Brazilian Northeast, are presented in Table 2.

Table 2. Daily averages of the radiation balance components for the mixed agro-ecosystems of the study semi-arid area inside Petrolina (PE), Northeast Brazil: global solar radiation (R_G), reflected solar radiation (R_R); atmospheric emitted long-wave radiation (RL_a); and surface emitted long-wave radiation (RL_s).

DOY/Mean	R_G (MJ m^{-2} d^{-1})		R_R (MJ m^{-2} d^{-1})		RL_a (MJ m^{-2} d^{-1})		RL_s (MJ m^{-2} d^{-1})	
DOY	IC	NV	IC	NV	IC	NV	IC	NV
025	24.13	24.23	4.59	4.61	34.70	34.67	42.87	42.88
153	19.99	19.89	3.69	3.70	32.02	32.01	39.29	39.22
217	19.31	19.20	3.63	3.65	32.96	32.98	39.69	39.65
265	23.92	23.90	4.67	4.81	34.87	34.89	44.16	44.16
Mean	**21.84**	**21.81**	**4.15**	**4.19**	**33.64**	**33.64**	**41.50**	**41.48**

*IC: Irrigated Crops; NV: Natural Vegetation; DOY: Day of the Year

R_G, considered as the radiation (directly or indirectly) from the sun, integrated over all wavelengths in the shortwave interval, presented seasonal variations along the year 2014, however with similar values in irrigated and natural vegetation areas. The highest values occurred in DOY 025, coinciding with the rainy period, while the smallest ones were in August (DOY 217).

The annual trend of R_R followed that for R_G, but its values were also affected by the soil moisture conditions, without significant differences between the agro-ecosystem types. The solar radiation absorbed by the surfaces is converted into heat energy. By several processes, including emission, they lose this energy, as longwave radiation.

The atmosphere absorbs the emitted longwave radiation from the surface (RL_s) or loses it into space. In general, RL_s presented seasonal variations, according to R_G levels, but with less dependence on the agro-ecosystem type when compared with R_R. Part of RL_s finds its way back to the surface as emitted longwave radiation from the atmosphere (RL_a).

RL_a is dependent on T_a, and on the concentration of carbon dioxide, water vapor and ozone. RL_s values stayed always above those for RL_a, by 20% in January (DOY 025) and 27 % in August (DOY 217), independently of the surface type. As RL_s was usually greater than RL_a, the net longwave radiation represented an energy loss from the semi-arid agro-ecosystems to the lower atmosphere.

Taking into account all components from Table 2, the net radiation (R_n) represents the difference between incoming and outgoing radiation of both short and long wavelengths. The fraction of R_G transformed into R_n, ranged from 41% (DOY 217) to 47% (DOY 025), averaging 45%, independently of the agro-ecosystem type. This is in agreement with field measurements in the semi-arid region of Brazil[19], and with studies involving other agro-ecosystems[35-36], which give additional confidence to the remote sensing methods tested here for the radiation and energy balance components acquirements on large-scales by using Landsat 8 satellite images and agrometeorological stations.

By using interpolated data of R_G and T_a from the agrometeorological stations showed in Fig. 1 together with α_0 images on a daily scale, the slob equation was applied to retrieve the large-scale R_n values[19] (Fig. 5).
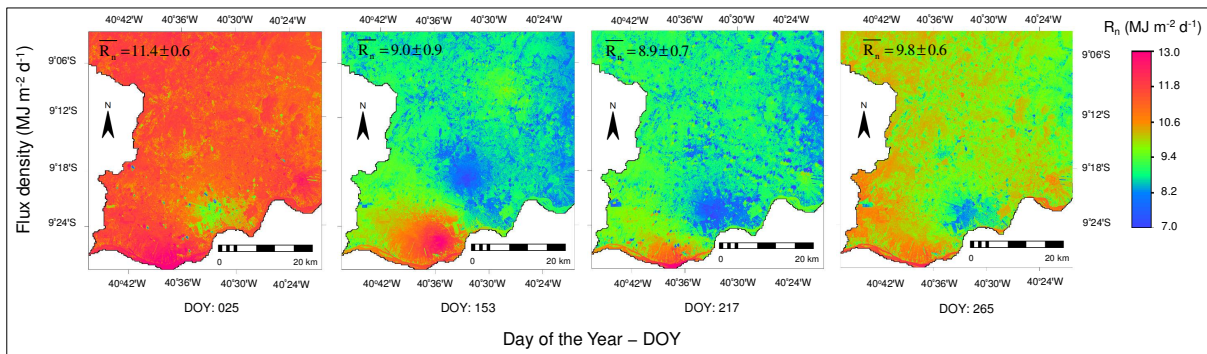

Figure 5. Spatial distribution for the net radiation (R_n) daily values of the semi-arid study area inside Petrolina (PE) municipality, Brazilian Northeast. Overbars mean average pixel values.

In general, there are no clear distinctions between the R_n pixel values from irrigated and from natural vegetation areas. In addition, there are no large spatial differences with the standard deviation (SD) values ranging from 0.6 to 0.9 MJ m^{-2} d^{-1}. The strong dependence of R_n is on R_G as one can see that the largest mean R_n values for DOY 025 and 265 corresponded to the highest ones of R_G (see Fig. 5 and Table 2). During these last periods, one can clearly see the lowest R_n values in the southern part of the semi-arid study area, where is located the Petrolina city, close to the São Francisco River.

It is clear from Fig. 5 that one cannot separate the R_n values from irrigated crops and from natural vegetation in the Brazilian semiarid mixed agro-ecosystems. Then, differences among them would arise when considering the energy partition into latent (λE), sensible (H), and ground (G) heat fluxes according to the thermohydrological conditions. These analyses are carried out in the next sub-section.

3.4 Large-scale energy balance

Acquiring ET throughout the SAFER algorithm and transforming it into energy units[16,22], λE was estimated. Considering G as a fraction of R_n and H as residue in energy balance equation, all of these energy balance components could be spatially determined[22].

Fig. 6 presents the spatial distribution of the daily values for λE, G and H in the semi-arid study area inside the Petrolina municipality, Pernambuco (PE) state, Northeast of Brazil, for each day of the year (DOY), involving different thermohydrological conditions along 2014.
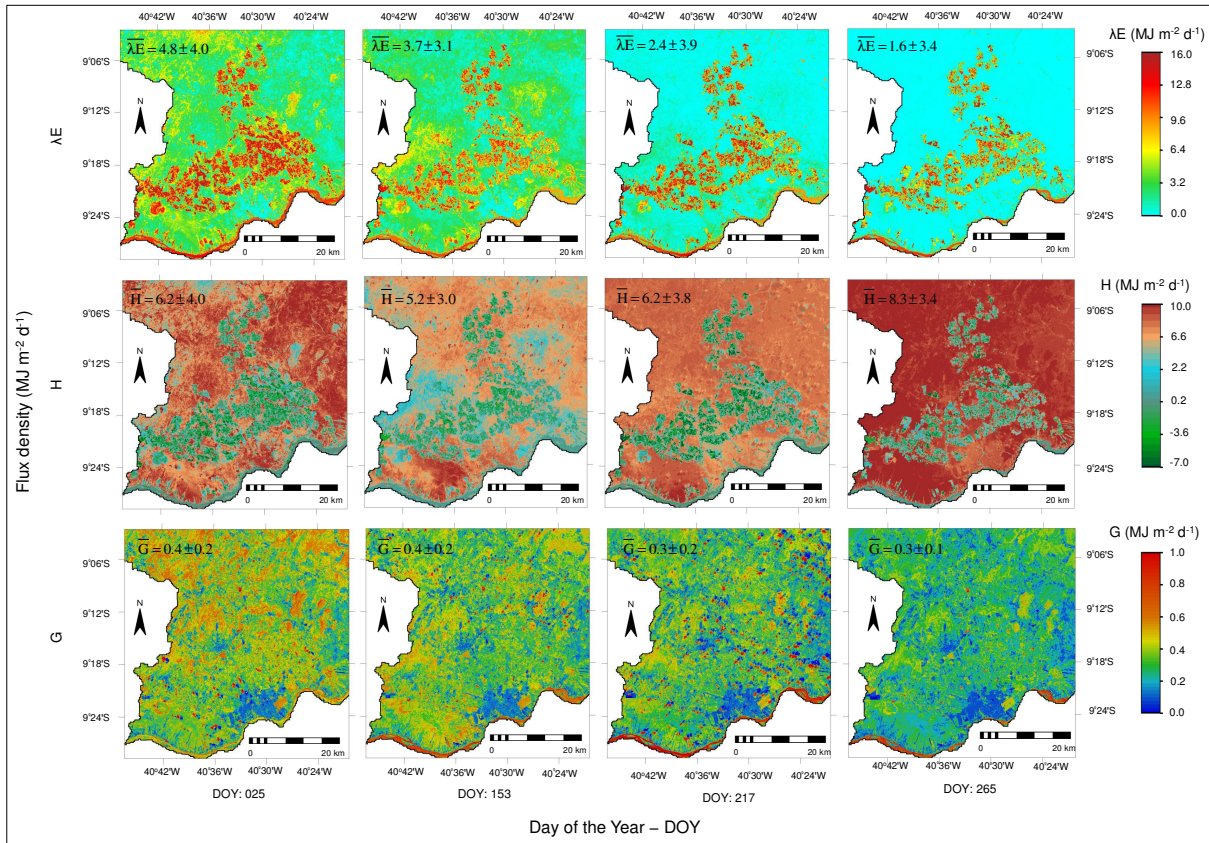
Figure 6. Spatial distribution of the daily values for the energy balance components in the semi-arid study area inside Petrolina (PE) municipality, Brazilian Northeast. Latent heat flux (λE); sensible heat flux (H); and ground heat flux (G). Overbars mean average pixel values.

Clearly one can distinguish irrigated areas from natural vegetation by the highest λE pixel values according to the period of the year, mainly when looking for the image of DOY 265, which represents the driest period condition. In some places, λE was higher than R_n, condition which represents very well irrigated plots (see Fig. 5 and 6). Because the largest fractions of the available energy used as sensible heat fluxes (H), during this driest conditions of the year (DOY 265), between August and October, the natural vegetation presented the lowest λE pixel values (bluish λE pixels), while the irrigated fields showed the highest ones (reddish λE pixels). Stomata of the natural species close under these conditions, limiting transpiration and photosynthesis, while, in general, irrigation intervals in crops are short (daily irrigation), reducing the heat losses to the atmosphere. The largest average λE is in January (DOY 025), because the joint effect of the rains and irrigation together with high atmospheric demand (see Fig. 3 and 6). During this time of the year, the hydrological large-scale soil moisture uniformity makes "Caatinga" having λE rates similar to those from irrigated crops and even higher in some occasions. Intermediate λE values in natural vegetation occurred after this period (DOY 153), because the previous rains still kept the natural ecosystem wet and green.

By H, also one can distinguish irrigated areas from "Caatinga" species by the their lowest values in relation to irrigation conditions, which was even negative in cropped areas, meaning heat horizontal advection from the warmer natural vegetation at the vicinities of irrigated plots, reaching to -7 MJ m^{-2} d^{-1} in the darker green areas. The largest positive H values corresponded to the lowest λE ones in the image of DOY 265, while the lowest average H values were soon after the rainy period (DOY 153), related to the joint effect of low R_G levels together with high soil moisture.

G was the energy balance parameter that presented very little differences among the different Brazilian semi-arid agro-ecosystems. In the case of this energy balance component, its values were too low, confirming that in most cases they approach to zero at the daily scale[16]. Few areas presented positive daily values reaching to around 1.0 MJ m^{-2} d^{-1}.

However, one can see the lowest G values in the southern part of the study area, where is located the Petrolina (PE) city, close to the São Francisco River, in all the images.

In relation to the spatial variations of the energy balance components, the lowest SD for λE and H were soon after the rainy season. Under these conditions, the soil moisture in the root zone of both irrigated crops and natural vegetation was still high but under low R_G levels (see Fig. 3 and 6), situation represented by image of DOY 153 (June 2014). G was the energy balance component, which presented the lowest spatial variation, although the slightly lower SD happened during the driest conditions of DOY 265, while for the other periods SD values were equal.

Considering the vegetation classification into irrigated crops (IC) and natural vegetation (NV) by using Eq. 16, and the threshold r_s limits[25], Table 3 shows the daily average energy partition into λE, H and G for these two kinds of agro-ecosystems, under different thermohydrological conditions in the study semi-arid region inside Petrolina (PE) municipality, Northeast of Brazil.

Table 3. Daily averages of the energy balance components for the mixed agro-ecosystems inside the study semi-arid area of Petrolina (PE), Northeast Brazil: latent heat flux (λE), sensible heat flux (H); soil heat flux (G); and evaporative fraction (E_f).

DOY/Mean	λE (MJ m^{-2} d^{-1})		H (MJ m^{-2} d^{-1})		G (MJ m^{-2}d^{-1})		E_f (-)	
DOY	IC	NV	IC	NV	IC	NV	IC	NV
025	7.77	4.25	3.21	6.77	0.39	0.39	0.71	0.39
153	6.32	3.22	2.35	5.41	0.36	0.35	0.73	0.37
217	5.69	1.75	2.91	6.80	0.35	0.33	0.66	0.20
265	7.88	0.36	1.79	9.20	0.29	0.26	0.81	0.04
Mean	**6.92**	**2.40**	**2.57**	**7.05**	**0.35**	**0.33**	**0.73**	**0.25**

*IC: Irrigated Crops; NV: Natural Vegetation; DOY: Day of the Year

The lowest λE average value for IC was at the start of August (DOY 217), while the highest one was during the driest natural conditions of DOY 265 (September), producing an evaporative fraction, [$E_f = λE/(R_n-G)$], from 0.66 to 0.81, respectively. For NV, the lowest λE average value was in September (DOY 265), and the largest one happened in January (DOY 025), being the E_f values between 0.04 and 0.39 for these periods, respectively. The characteristics of the "Caatinga" natural ecosystem were manifested by λE low values outside the rainy season. Under irrigation conditions, the largest E_f happened on occasions of the highest heat advection from the natural drier species to the irrigated plots.

Considering the whole year, H mean pixel values for natural vegetation was almost three times larger than those for irrigated crops. On average, H reached to 94% of R_n in September (DOY 265) for NV, while the corresponding fraction was only 18% for IC. The additional energy source from the natural species during this period, contributed to an increment of the water consumption by irrigated crops.

Despite being recorded G values reaching as far as 1.0 MJ m^{-2} d^{-1} through Fig. 6 in some areas, its averages for both IC and NV were too low, with G/R_n fractions ranging from 3 to 4%, without distinction between the season of the year neither agro-ecosystems.

Considering the different thermohydrological conditions along the year 2014 in the semi-arid study area of Petrolina (PE), Brazilian Northeast, in average, the ratios R_n/R_G, $λE/R_n$, H/R_n and G/R_n were respectively 0.45, 0.70, 0.26 and 0.04 for irrigated crops, while the corresponding ratios for natural vegetation were 0.45, 0.25, 0,72 and 0.03. These fractions are relevant when considering the effects of the rapid land-use changes on the radiation and energy balance components along the years.

4. CONCLUSIONS

The coupled use of Landsat 8 (L8) images and agrometeorological stations allowed the quantification and analyses of the radiation and energy balances on a large-scale along the year 2014 under different thermohydrological semi-arid conditions of the Petrolina municipality, Pernambuco state, Northeast Brazil. Net radiation (R_n) was most strongly

influenced by the solar radiation levels than by the characteristics of the different agro-ecosystems types. It was demonstrated that the daily values of latent (λE), sensible (H) and ground (G) heat fluxes can be estimated for irrigated crops and natural vegetation from instantaneous measurements of the visible, near infra-red and thermal radiations from the L8 sensor, throughout the application of the SAFER and SUREAL algorithms. The mean fractions of the λE, H and G to R_n were 70, 26 and 4% and 25, 72 e 3%, considering irrigated crops and natural vegetation, respectively. In some occasions, inside the irrigated areas, it was evidenced heat fluxes coming from the natural dryer areas at the vicinities of agricultural crops, promoting λE higher than R_n and negative H values. These large-scale analyses can contribute for the monitoring of the land use and climate changes effects in the Brazilian semi-arid region. The confidence of the modelling success here gives more confidence for using the algorithms in other environments around the world, which probably will need only calibrations of the original equations.

ACKNOWLEDGEMENTS

REFERENCES

[1] Teixeira, A. H. de C., "Determining regional actual evapotranspiration of irrigated and natural vegetation in the São Francisco river basin (Brazil) using remote sensing and Penman-Monteith equation, ". Rem. Sens., 2, 1287−1319 (2010).

[2] Miralles, D.G., Holmes, T.R.H., De Jeu, R.A.M., Gash, J.H., Meesters, A.G.C.A. and Dolman, A.J., "Global land-surface evaporation estimated from satellite-based observations,". Hydrol. Earth Syst. Sci., 15, 453−469 (2011).

[3] Anderson, M.C., Kustas, W.P., Alfieri, J.G., Gao, F. and Hain, C., "Mapping daily evapotranspiration at Landsat spatial scales during BEAREX'08 field campaign,". Adv. Water Res., 50,162−177 (2012).

[4] Pôças, I., Cunha, M., Pereira, L.S. and Allen, R.G., "Using remote sensing energy balance and evapotranspiration to characterize montane landscape vegetation with focus on grass and pasture lands,". Int. J. Appl. Earth Obs. Geoinf., 21,159−172 (2013).

[5] Bastiaansssen, W.G.M., Menenti, M., Feddes, R.A., Roerink, G.J. and Holtslag, A.A.M., "A remote sensing surface energy balance algorithm for land (SEBAL) 1. Formulation,". J. Hydrol., 212−213, 198−212 (1998).

[6] Roerink, G.J., Su, Z. and Menenti, M. "S-SEBI: A simple remote sensing algorithm to estimate the surface energy balance,". Phy. Chem. Earth, 25, 147−157 (2000).

[7] Su, Z., "The Surface Energy Balance System (SEBS) for estimation of turbulent heat fluxes,". Hydrol. Earth Syst. Sci., 6, 85−99 (2002).

[8] Kustas, W.P. and Norman, J. M., "Evaluation of soil and vegetation heat flux predictions using a simple two-source model with radiometric temperatures for partial canopy cover,". Agric. For. Meteorol., 94, 13−29 (1999).

[9] Norman, J.M., Kustas, W.P., Prueger, J.H. and Diak, G.R., "Surface flux estimation using radiometric temperature: A dual-temperature-difference method to minimize measurement errors,". Water Resour. Res., 36, 2263−2274 (2000).

[10] Norman, J. M., Anderson, M.C., Kustas, W.P., French, A.N., Mecikalski, J., Torn, R., Diak, G.R., Schmugge, T.J. and Tanner, B.C.W., "Remote sensing of surface energy fluxes at 101-m pixel resolutions,". Water Resour. Res., 39, SWC91−SWC917 (2003).

[11] Kalma, J.D. and Jupp, D.L.B., "Estimating evaporation from pasture using infrared thermometry: Evaluation of a one-layer resistance model,". Agric. Forest Meteorol., 51, 223−246 (1990).

[12] Cleugh, H.A., Leuning, R., Mu, Q. and Running, S.W., "Regional evaporation estimates from flux tower and MODIS satellite data,". Rem. Sens. Env., 106, 285−304 (2007).

[13] Allen, R.G., Tasumi, M., Morse, A., Trezza, R, Wright, J.L. and Bastiaanssen, W.G.M., "Satellite-based energy balance for mapping evapotranspiration with internalized calibration (METRIC)—Applications,". J. Irr. Drain. Eng. ASCE 133, 395−406 (2007).

[14] Teixeira, A.H. de C., Bastiaanssen, W.G.M., Ahmad, M–ud–D and Bos, M.G., "Reviewing SEBAL input parameters for assessing evapotranspiration and water productivity for the Low-Middle São Francisco River basin, Brazil Part A: Calibration and validation,". Agric. For. Meteorol. 149, 462−476 (2009a).

[15] Teixeira, A.H. de C., Bastiaanssen, W.G.M., Ahmad, M–ud–D and Bos, M.G., "Reviewing SEBAL input parameters for assessing evapotranspiration and water productivity for the Low-Middle São Francisco River basin, Brazil Part B: Application to the large scale,". Agric. For. Meteorol. 149, 477–490 (2009b).

[16] Teixeira, A.H. de C., Hernandez, F.B.T., Lopes, H.L., Scherer-Warren, M. and Bassoi, L.H., A Comparative Study of Techniques for Modeling the Spatiotemporal Distribution of Heat and Moisture Fluxes in Different Agroecosystems in Brazil. In: George G. Petropoulos. (Org.). Remote Sensing of Energy Fluxes and Soil Moisture Content. 1ed.Boca Raton, Florida: CRC Group, Taylor and Francis, 169–191 (2014a).

[17] Vanhellemont, Q. and Kevin Ruddick, K., "Turbid wakes associated with offshore wind turbines observed with Landsat 8,". Rem. Sens. Env., 145, 105–115 (2014).

[18] Teixeira, A.H. de C., Water productivity assessments from field to large scale: a case study in the Brazilian semi-arid region; LAP Lambert Academic Publishing: Saarbrücken, Germany, 226p. (2009).

[19] Teixeira, A.H. de C., Bastiaanssen, W.G.M., Ahmad, M–ud–D, Bos, M.G. and Moura, M.S.B., "Analysis of energy fluxes and vegetation-atmosphere parameters in irrigated and natural ecosystems of semi-arid Brazil,". J. Hydrol., 362, 110–127, (2008).

[20] Allen, R.G., Hartogensis, O. and de Bruin, H.A.R., "Long-wave radiation over alfafa during the RAPID field campaign in southern Idaho,". Research Report, Kimberly, Univ. of Idaho, Id (2000).

[21] Teixeira, A.H. de C., Victoria, D. de C., Andrade, R.G., Leivas, J.F., Bolfe, E.L. and Cruz, C.R., "Coupling MODIS images and agrometeorological data for agricultural water productivity analyses in the Mato Grosso state, Brazil,". Proc. SPIE 9239, 92390 (2014b).

[22] Teixeira, A.H. de C., Hernandez, F.B.T., Andrade, R.G., Leivas, J.F. and Bolfe, E.L., "Energy balance with Landsat images in irrigated central pivots with corn crop in the São Paulo State, Brazil,". Proc. SPIE 9239, 92390, (2014c).

[23] Allen, R.G., Pereira, L.S., Raes, D. and Smith, M., Crop Evapotranspiration: Guidelines for Computing Crop Water Requirements; Food and Agriculture Organization of the United Nations: Rome, Italy (1998).

[24] Raupasch, M.R., "Combination theory and equilibrium evaporation,". Q. J. Roy. Meteor. Soc. 127, 1149–1181, (2001).

[25] Teixeira, A. H. de C., "Determination of surface resistance to evapotranspiration by remote sensing parameters in the semi-arid region of Brazil for land-use change analyses,". IAHS Press, Wallingford, UK, 352, 167–170 (2012).

[26] Li, S.-G., Eugster, W., Asanuma, J, Kotani, A., Davaa, G., Oyunbaatar, D. and Sugita, M., "Energy partitioning and its biophysical controls above a grazing steppe in central Mongólia," Agric. For. Meteorol., 137, 89–106 (2006).

[27] van Dijk, A.I.J.M., Bruijnzeel, L.A. and Schellekens, J., "Micrometeorology and water use of mixed crops in upland West Java, Indonesia," Agric. For. Meteorol. 124, 31–49 (2004).

[28] Monteith, J.L. and Unsworth, M.H., Principles of environmental physics. Arnold: London, 291p., (1990).

[29] Oguntoyinbo, J.S., "Reflection coefficient of natural vegetation, crops and urban surfaces in Nigeria,". Q. J. Roy. Meteor. Soc. 96, 430–441, (1970).

[30] Pinker, R.T., Thompson, O.E. and Eck, T.F., "The albedo of a tropical evergreen forest,". Q. J. Roy. Meteor. Soc., 106, 551–558, (1980).

[31] Shuttleworth, W.J., "Evaporation from Amazonian rain forest,". Proc. Roy. Soc. Lond. B Biol. Sci. 233, 321–346 (1988).

[32] Lobell, D.B. and Asner, G.P., "Moisture effects on soil reflectance,". Soil Sci. Soc. Am. J. 66, 722–727 (2002).

[33] Yuan, M., Zhang, L., Gou, F., Su, Z., Spiertz, J.H.J., Werf, W. van der. 2013. Assessment of crop growth and water productivity for five C3 species in the semi-arid Inner Mongolia,". Agric. Water Manage., 122, 28–38.

[34] Wang, Ma, M., Huang, G., Veroustraete, F., Zhang, Z., Song, Y. and Tan, J, ". Vegetation primary production estimation at maize and alpine meadow over the Heihe River Basin, China,". Int. J. Appl. Earth Obs. Geoinf., 17, 94–101 (2012).

[35] Yunusa, I.A.M., Walker, R.R. and Lu, P., "Evapotranspiration components from energy balance, sapflow and microlysimetry techniques for an irrigated vineyard in inland Australia," Agric. For. Meteorol. 127, 93–107 (2004).

[36] Hughes, C. E., Kalma, J. D., Binning, P., Willgoose, G. R. and Vertzonis, M., "Estimating evapotranspiration for a temperate salt marsh Newcastle, Australia,". Hydrol. Process. 15, 957–975 (2001).